Nonlocal pseudopotentials in complex band-structure and photoemission calculations

A. Bödicker and W. Schattke
Institut für Theoretische Physik, Leibnizstraße 15, D-24118 Kiel, Germany
(Received 13 August 1996; revised manuscript received 30 September 1996)

Based on a recently proposed localization procedure, a nonlocal pseudopotential scheme is derived to calculate potential coefficients $V_{\vec{G}\vec{G}'}(\vec{k})$ which can be decomposed into terms, each being quadratic in $\vec{k}$ and multiplied by a function of $(\vec{G}-\vec{G}')$, thus making them applicable to some important cases where local potential coefficients are required. Electronic structure calculations for semiconductors are in agreement with well-known semiempirical local pseudopotential band structures, as shown for GaAs. Nevertheless, the potential may significantly deviate from the semiempirical results. In order to test wave functions and transition probabilities, we prove the success of the procedure in a more troublesome case, i.e., applying it to a transition-metal compound as the experimentally well-investigated layered crystal $TiSe_2$, which up to now was not treated with a pseudopotential. Photoemission spectra within the one-step model are presented using Pendry's method of complex band-structure calculation. The latter formalism had to be slightly generalized for the quasilocal properties of the potential. The agreement of the spectra with experimental data shows this method to be a reliable and practical tool to use nonlocal pseudopotentials for conduction-band wave functions of electron spectroscopies. [S0163-1829(97)04408-1]

I. INTRODUCTION

The widely used empirical local pseudopotentials[1–11], as, e.g., introduced by Cohen and Bergstresser,[12] are attractive because of their simplicity, relying only on a few elements derived from fitting to optical data. The property of being local allows for a reduction of computational efforts. This is not relevant in standard band-structure determinations, but it is helpful in tasks which need a band structure computation as a single and often repeated step,[13] and crucially arises in the computation of complex band structures as needed, e.g., in the calculation of the photoemission spectra[9] or of the spectra of elastically diffracted electrons at very low energies (VLEED).[6,8,11] Especially in the latter case the scattering states are conveniently obtained via Pendry's technique to solve the inverse problem for the complex band structure, which in its simplest form requires a local potential.[14]

In view of these advantages, two drawbacks prove to be cumbersome in actual applications: first, the lack of an *ab initio* base, and, second, the problem of generating the potential coefficients. Apart from the tabulated zinc-blende potentials, suitable coefficients have to be found by an unsatisfying trial and error procedure. Depending on the system under consideration, it may not converge at all.

In contrast to this situation, a well-tested technique for the construction of *ab initio* atomic pseudopotentials exists.[15–17] They depend principally on angular momentum in a nonlocal way, which would prohibit an application to the above class of problems. However, recently a method was presented to convert these potentials to a local Hamiltonian atomic potential.[18] It was intended to serve Monte Carlo simulations. We could benefit from that development in constructing crystal potentials which, after a simple generalization of Pendry's method, are conveniently applied to electron spectroscopy. With a straightforward determination of the potential coefficients in a plane-wave basis,[19] we are able to generate a potential for layered dichalcogenides, hitherto not successfully treated in the pseudopotential scheme.

In this paper we report our applications of the pseudopotential of Bachelet, Ceperly, and Chiocchetti to GaAs for the reason of comparing it with the standard local potential, and to the layered crystal $TiSe_2$ for showing its success in treating complex systems. We briefly outline the conversion from a nonlocal to a quasilocal potential of the solid.

II. METHOD OF CALCULATION

The matrix elements of the separable generalized norm-conserving pseudopotentials by Hamann[17] are calculated as

$$\langle\Phi_1|V|\Phi_2\rangle=\sum_{l=0}^{\infty}\sum_{m=-l}^{l}\int d\vec{r}\int d\vec{r}\,'\,\Phi_1^*(\vec{r})Y_{lm}(\hat{r})V_l(r)\times\frac{\delta(r-r')}{r^2}Y_{lm}^*(\hat{r}')\Phi_2(\vec{r}\,'). \quad (1)$$

This potential is local in r and nonlocal in θ and ϕ. Replacing Eq. (1), Bachelet, Ceperley, and Chiocchetti introduced a local pseudopotential matrix[18]

$$\langle\Phi_1|V|\Phi_2\rangle=\int d\vec{r}\int d\vec{r}\,'\langle\Phi_1|\vec{r}\,'\rangle\delta(\vec{r}-\vec{r}\,')\times\left[v(r)-\frac{1}{2}\nabla a(r)\nabla+b(r)\frac{\mathbf{L}^2}{2r^2}\right]\langle\vec{r}|\Phi_2\rangle, \quad (2)$$

which reproduces the action of the nonlocal pseudopotentials with respect to the angular-momentum dependence. Outside the core, the radial functions $a(r)$ and $b(r)$ must vanish, and $v(r)$ should asymptotically vanish as $-Z_v/r$ (Z_v is the valence charge). The three unknown functions can be determined by requiring that the three lowest l radial eigenfunctions $u_l(r)$ and eigenvalues E_l of the radial Schrödinger

equation are identical for both pseudopotentials. This restriction leads to the following system of three differential equations:

$$\left[a\frac{d^2}{dr^2}-(a+b)\frac{l(l+1)}{r^2}+\frac{da}{dr}\left(\frac{d}{dr}-\frac{1}{r}\right)-2(v-V_l)\right]u_l=0, \tag{3}$$

with V_l being the norm-conserving pseudopotential by Hamann.[17] Choosing the simple analytic form $a(r)=a_0\exp(-(r/r_c)^k)$, $a_0=0.9$, $r_c=1.0$, and $k=2$, proposed in Ref. 18, Eq. (3) for $l=0$ and 1 is used to determine b and v:

$$v=a\frac{u_0''}{2u_0}+a'\left[\frac{u_0'}{2u_0}-\frac{1}{2r}\right]+V_0,$$

$$b=-a+a\frac{r^2u_l''}{l(l+1)u_l}+a'\frac{r^2u_l'-ru_l}{l(l+1)u_l}-2\frac{[v-V_l]r^2}{l(l+1)}.$$

We adapted the atomic pseudopotential to the solid by calculating the atomic matrix elements $\langle\vec{k}+\vec{G}|V|\vec{k}+\vec{G}'\rangle=V_{\vec{G}\vec{G}'}(\vec{k})$ in a basis of plane waves with Bloch vector $\vec{k}$ and reciprocal-lattice vector $\vec{G}$. For $\vec{G}\neq\vec{G}'$, one obtains

$$\begin{aligned}V_{\vec{G}\vec{G}'}(\vec{k})=&\,v_{\Delta\vec{G}}+\vec{K}\cdot\vec{K}'a_{\Delta\vec{G}}+\vec{K}'^2(u^{(1)}_{\Delta\vec{G}}-u^{(2)}_{\Delta\vec{G}})\\&+[\vec{K}'\cdot\Delta\vec{G}]^2(-u^{(1)}_{\Delta\vec{G}}+3u^{(2)}_{\Delta\vec{G}})/\Delta\vec{G}^2\\&+\vec{K}'\cdot\Delta\vec{G}(-2u^{(2)}_{\Delta\vec{G}}),\end{aligned} \tag{4}$$

where $(a_G,u_G^{(1)},u_G^{(2)},v_G)$ are the threedimensional Fourier transforms of $1/2(a(r),\ b(r),\ b(r)r\cos\theta/(Gr^2),\ 2v(r))$ with a polar angle θ measured in a coordinate system with $\vec{G}$ being parallel to the z axis, $\vec{K}^{(\prime)}=\vec{k}+\vec{G}^{(\prime)}$, and $\Delta\vec{G}=\vec{G}'-\vec{G}$. Because of rotational invariance the various coefficients depend only on the absolute value of $\vec{G}$. For $\vec{G}=\vec{G}'$, the formula simplifies to

$$V_{\vec{G}\vec{G}}=(\vec{k}+\vec{G})^2\left(a_0+\frac{2}{3}u_0^{(1)}\right)+E_{\text{shift}}. \tag{5}$$

E_{shift} pins the valence band maximum to the energy zero. These plane-wave matrix elements previously have been used to accelerate the Car-Parinello iteration scheme.[19]

III. APPLICATION TO GAAS

Once the atomic potentials have been determined, it is straightforward to solve for the energy-band spectrum, using the following elements of the Hamiltonian matrix:

$$H_{\vec{G}\vec{G}'}(\vec{k})=\tfrac{1}{2}(\vec{k}+\vec{G})^2\delta_{\vec{G}\vec{G}'}+SV_{\vec{G}\vec{G}'}(\vec{k}), \tag{6}$$

where $V_{\vec{G}\vec{G}'}(\vec{k})$ now comprises the sum over the constituting atomic potentials, Eqs. (4) and (6). The strength S of the potential is introduced as a parameter, the only one of this theory. It affects the overlap between the atomic electronic densities. Having calculated pseudopotential coefficients for the atoms, the overlap usually arises as being too small. Increasing the overlap is achieved by reducing the strength of the potential. The rearrangement of the electronic densities of free atoms to the electronic density in a crystal could be principally obtained by self-consistency loops. In a short cut, we estimated the parameter S *a posteriori*. For galliumarsenide, $S=0.719$ gives the best agreement with former band structure calculations.[12,20,21] Note that this is opposite to the behavior of atomic orbitals of an atomic all-electron calculation, which usually contract upon being transfered to the solid. In a tight-binding calculation the overlap integrals determined, e.g., with the widely used Clementi-Roetti data,[22] overestimate the interaction range, because the electronic environment of the crystal compresses the orbitals.[9] Here, in the pseudopotential approach, the orbitals expand. This seems to be a consequence of the calculational method. Using only one parameter represents remarkable progress compared with the empirical pseudopotential methods, where all local coefficients had to be fitted to optical data,[12] and where nonlocal correction terms were added to the local potentials.[20,21]

TABLE I. Pseudopotential coefficients for arsenic. Units are $(2\pi/a)^2$ (a is the lattice constant) for the first column, Hartree for the next column, and Hartree (Bohr)^2 for the last three columns.

G^2	v_G	a_G	$u_G^{(1)}$	$u_G^{(2)}$
0		−0.016 44	0.007 72	0.000 00
3	−0.116 79	−0.012 69	0.007 62	0.003 03
4	−0.069 21	−0.011 64	0.006 58	0.002 79
8	−0.003 46	−0.008 23	0.003 48	0.002 03
11	0.010 10	−0.006 35	0.002 01	0.001 59
12	0.012 32	−0.005 82	0.001 64	0.001 47
16	0.016 09	−0.004 12	0.000 60	0.001 08
19	0.015 89	−0.003 18	0.000 18	0.000 86
20	0.015 55	−0.002 92	0.000 08	0.000 80
24	0.013 36	−0.002 06	−0.000 13	0.000 61

Tables I and II list the pseudopotential coefficients for arsenic and for gallium. The energy shift $v_0=E_{\text{shift}}$ is not displayed, because it depends on the number of plane waves used and on the cutoff radius for the potential parameters. The minimum cutoff radius of $\sqrt{24}$ to obtain an adequate (valence) band structure becomes larger than $\sqrt{11}$ of the empirical pseudopotential calculations[12] because the number of coefficients of a Fourier expansion usually exceeds the num-

TABLE II. Pseudopotential coefficients for gallium, for units, see Table I.

G^2	v_G	a_G	$u_G^{(1)}$	$u_G^{(2)}$
0		−0.016 44	0.006 99	0.000 00
3	−0.053 05	−0.012 69	0.007 30	0.002 84
4	−0.024 37	−0.011 64	0.006 39	0.002 64
8	0.013 75	−0.008 23	0.003 37	0.001 95
11	0.020 08	−0.006 35	0.001 73	0.001 52
12	0.020 80	−0.005 82	0.001 28	0.001 40
16	0.020 45	−0.004 12	−0.000 05	0.000 97
19	0.018 51	−0.003 18	−0.000 66	0.000 72
20	0.017 73	−0.002 92	−0.000 80	0.000 65
24	0.014 33	−0.002 06	−0.001 11	0.000 42

TABLE III. Local pseudopotential coefficients in eV.

	V_3^S	V_8^S	V_{11}^S	V_3^A	V_4^A	V_{11}^A
This paper	−3.32	0.20	0.59	1.25	0.88	0.19
Ref. 12	−3.13	0.14	0.82	0.95	0.68	0.14

ber obtained by minimizing a set of fit parameters. Extending the cutoff radius does not change the band structure up to 30 eV appreciably.

An interesting simplification arises from the restriction to the bare local part of our potential, i.e., to the first term in Eq. (4), leading to minor deviations in the conduction band structure only. Table III shows the converted local part of the pseudopotential coefficients of this paper to be directly compared with those of Ref. 12.

Figure 1 shows the quasilocal pseudopotential band structure (solid lines) in comparison with the semiempirical band structure by Cohen and Bergstresser[12] (dashed lines). We have used 137 plane waves in both calculations. Increasing the number of plane waves does not change the bands in the displayed energy region. The comparison of the two band structures obtained from differently determined pseudopotentials shows good agreement below the Fermi level. The optical gap of 1.5 eV is achieved in both calculations. Comparing the conduction band structures, the differences are no longer negligible. This and differing wave functions will influence matrix elements and should lead to differences in theoretical electron spectroscopy.

IV. APPLICATION TO $TiSe_2$

As a prototype of a system withstanding a semiempirical pseudopotential approach, we have chosen a compound from the class of layered transition-metal dichalcogenides, $TiSe_2$.[23] The crystal structure may be described as a stack of identical layers, loosely bound to each other across a van der Waals gap. Each layer consists of a sheet of titanium atoms, sandwiched between two sheets of selenium atoms. The atomic pseudopotential coefficients of titanium and selenium have been determined using the calculation scheme outlined above, restricting the angular momentum to $l=2$ for the cation and to $l=1$ for the anion.

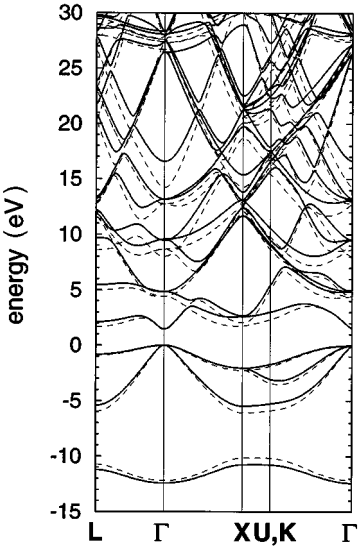

FIG. 1. Band structure of GaAs calculated with the pseudopotential coefficients of this paper (solid lines) and from Ref. 12 (dashed lines).

In order to test the potential by its wave functions and matrix elements, photoemission spectra in the ΓA direction have been computed and compared with experimental data[24,25] and with former calculations.[25] The photoemission theory is based on the single-particle one-step model outlined in Ref. 26. Only the final states are determined from the quasilocal potential. The basis of the initial states is calculated within an empirical linear combination of atomic orbitals (LCAO) representation to account for the tight binding. The surface of the half-space is properly taken into account by determining the layer and wave-vector-resolved Green's function applying a highly convergent renormalization scheme.[27] The final state, a time inverse low-energy electron-diffraction (LEED) state, is taken as a superposition of bulk wave functions,

$$\Phi^*_{\mathrm{LEED}}=\sum_n t_n \sum_{\vec{G}} \alpha_{\vec{G}}^{(n)}(\vec{k}_n)\exp[-i(\vec{k}_n+\vec{G})\cdot\vec{r}] \qquad (7)$$

with coefficients t_n, being further decomposed into plane waves with coefficients $\alpha_{\vec{G}}^{(n)}$. Outside the crystal, the final state is written as a direct superposition of plane waves. The eigenfunctions of the Hamiltonian result from a calculation of the complex band structure, considering an energy-dependent imaginary part of the optical potential. In fact, we use two different descriptions of the Hamiltonian accounting for the special properties of initial and final states. The LCAO representation is a suitable tool to describe the rather localized valence electrons of the initial states. The conduction electrons representing the final states are free electron like, because they are forbidden by the Pauli principle from entering the immediate neighborhood of the ions already occupied by the valence electrons. The behavior of these nearly free electrons cannot be described by a localized (tight binding) basis but by a superposition of very few plane waves. In principle, the plane-wave basis could also be used for the initial states. But localized states require a very large number of plane waves increasing the valence states' computational efforts, which, however, should be kept low to leave space for the other parts of the photoemission code. Generally, the one-step model uses muffin-tin potentials, being adequate for metallic systems but failing in the case of covalently bound solids. One common procedure to meet these difficulties is to employ eigenstates of different Hamiltonians for the initial localized and final extended states, and to work on the $\vec{p}\cdot\vec{A}$ scheme of the matrix elements.[5,9,25,28]

To apply our quasilocal pseudopotential coefficients, the method proposed by Pendry[14] has to be generalized. For this purpose, the matrix equation

$$\sum_{\vec{G}'}\left[\left(\frac{1}{2}(\vec{k}+\vec{G})^2-E\right)\delta_{\vec{G}\vec{G}'}+SV_{\vec{G}\vec{G}'}(\vec{k})\right]\alpha_{\vec{G}}=0 \qquad (8)$$

is rewritten by introducing an intermediate variable $\vec{\beta}$, with $\beta_{\vec{G}}=(k_\perp+G_\perp)\alpha_{\vec{G}}$,

$$-\hat{A}\vec{\beta}-(\hat{B}-E\hat{1})\vec{\alpha}=k_\perp\hat{M}\vec{\beta},\quad \hat{1}\vec{\beta}-\hat{C}\vec{\alpha}=k_\perp\hat{1}\vec{\alpha},$$

where the matrices $\hat{A}$, $\hat{B}$, $\hat{C}$, and $\hat{M}$ do not depend on $k_\perp$, the surface perpendicular component of the wave vector $\vec{k}$. The matrix elements for $\Delta\vec{G}\neq 0$ are given by the following formulas:

$$\begin{aligned}A_{\vec{G}\vec{G}'}&=G_\perp(a_{\Delta\vec{G}}+\tfrac{1}{2}\delta_{\vec{G}'\vec{G}})+G'_\perp(u^{(1)}_{\Delta\vec{G}}-u^{(2)}_{\Delta\vec{G}})\\&\quad-G'_\perp(G'_\perp-G_\perp)^2(u^{(1)}_{\Delta\vec{G}}-3u^{(2)}_{\Delta\vec{G}})/\Delta\vec{G}^2\\&\quad-2(G'_\perp-G_\perp)u^{(2)}_{\Delta\vec{G}}-2(G'_\perp-G_\perp)(\vec{k}_\parallel+\vec{G}_\parallel)\\&\quad\cdot(\vec{G}'_\parallel-\vec{G}_\parallel)(u^{(1)}_{\Delta\vec{G}}-3u^{(2)}_{\Delta\vec{G}})/\Delta\vec{G}^2,\end{aligned}$$

$$\begin{aligned}B_{\vec{G}\vec{G}'}&=(\vec{k}_\parallel+\vec{G}'_\parallel)\cdot(\vec{k}_\parallel+\vec{G}_\parallel)(a_{\Delta\vec{G}}+\tfrac{1}{2}\delta_{\vec{G}'\vec{G}})\\&\quad+(\vec{k}_\parallel+\vec{G}'_\parallel)^2(u^{(1)}_{\Delta\vec{G}}-u^{(2)}_{\Delta\vec{G}})-2(\vec{k}_\parallel+\vec{G}'_\parallel)\\&\quad\cdot(\vec{G}'_\parallel-\vec{G}_\parallel)u^{(2)}_{\Delta\vec{G}}-[(\vec{k}_\parallel+\vec{G}'_\parallel)\cdot(\vec{G}'_\parallel-\vec{G}_\parallel)]^2\\&\quad\times(u^{(1)}_{\Delta\vec{G}}-3u^{(2)}_{\Delta\vec{G}})/\Delta\vec{G}^2,\end{aligned}$$

$$\begin{aligned}M_{\vec{G}\vec{G}'}&=a_{\Delta\vec{G}}+\tfrac{1}{2}\delta_{\vec{G}'\vec{G}}+u^{(1)}_{\Delta\vec{G}}-u^{(2)}_{\Delta\vec{G}}\\&\quad-(G'_\perp-G_\perp)^2(u^{(1)}_{\Delta\vec{G}}-3u^{(2)}_{\Delta\vec{G}})/\Delta\vec{G}^2,\end{aligned}$$

$$C_{\vec{G}\vec{G}'}=G'_\perp\delta_{\vec{G}\vec{G}'}.$$

In the case of $\Delta\vec{G}=0$ these formulas are shorter and simpler.

This transformation of Eq. (8) is possible because of the special form of the quasilocal pseudopotential coefficients, being at most, quadratic in $k_\perp$. A generalized eigenvalue problem for the momentum eigenvalues $k_\perp$ has to be solved. In order to fix the parameters S and E_{shift} for the conduction-band structure of $TiSe_2$, we calculated a target current spectrum (TCS) for $TiTe_2$ and compared it to experimental data. For the isoelectronic systems $TiTe_2$ and $TiSe_2$, the same potential strength S may be used. Values of $S=0.2$ and $E_{\text{shift}}=-2.8$ eV lead to satisfactory agreement between theoretical and experimental first derivatives of the TCS data. Comparing the conduction-band structures of $TiSe_2$ and $TiTe_2$ obtained with these parameters, the main difference is a simple shift of about 2.5 eV within the interesting energy region. Computing photoemission spectra of $TiSe_2$, it turns out that $E_{\text{shift}}=-1.8$ eV leads to even better agreement between calculated and experimental photoemission spectra. The strong reduction of the potential by the low value of S is associated with the higher-energy regime used here for the conduction states, as opposed to the GaAs example, where we focused on the valence states. It is to be expected that a local-density-approximation treatment would screen the deep atomic Ti potentials by the mainly occupied Se p states in the solid, thus further reducing the potential felt by the unoccupied, especially the Ti $3d$, states.

For the subsequent discussion of the photoemission, the valence part of the quasilocal pseudopotential band structure is of no importance. For completeness, we note some values of S and E_{shift} for that energy range. Taking the same S as for the excited states, the resulting valence bands have an

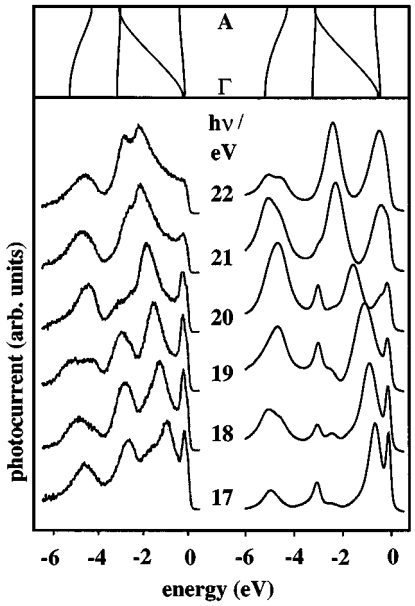

FIG. 2. Calculated (right side) and experimental (left side, taken from Ref. 24) surface normal photoemission spectra for $TiSe_2$. The plots of the photocurrent vs binding energy are characterized by the value of the photon frequency. The upper panel shows the ΓA valence band structure here repeated for the binding energy scales of both sets of spectra.

$E_{\text{shift}}=-13.5$ eV, i.e., the conduction bands have to be shifted by about 11.7 eV to higher energies to agree with the usual findings. However, in the ΓA direction the valence-band width of the more dispersive bands is too large, and the nondispersive bands are seen at somewhat higher energies. For $S=0.345$ and $E_{\text{shift}}=-13.1$ eV, the shape of the valence bands look more reasonable, but from an initially almost satisfying position the conduction bands now shift down by $-E_{\text{shift}}$. For higher S all bands flatten in the ΓA direction, losing their similarity with the known band structure. The Se-dominated bands mostly cover the valence regime, whereas the Ti states dominate in the conduction bands. The atomic pseudopotential seems to be more reliable for Se than for Ti. Like the potential strength S being reduced to much lower values because of the deep potential, here again this potential is responsible for the necessary high relative shift of the conduction bands to reach a reasonable position. This strong energy dependence of the parameters S and E_{shift} would require a kind of scissor operator if applied to photoemission. However, in view of our numerical program for the one-step model, here we rely on the LCAO representation of the valence bands which hitherto proved to reflect very accurately the actual positions of the valence bands.

Figure 2 shows the computed photoemission spectra in the ΓA direction. Because there appears to be almost no valence band crossing along the ΓA direction, the photoemission maxima can easily be assigned. Both peaks at the binding energy of -3 eV and near the Fermi level arise from the nearly nondispersive valence bands, and are derived from in-plane bonding orbitals, whereas the maximum dispersing from -0.8 to -3 eV is derived from bonds perpendicular to the surface. In Ref. 29 a discussion of matrix elements can be

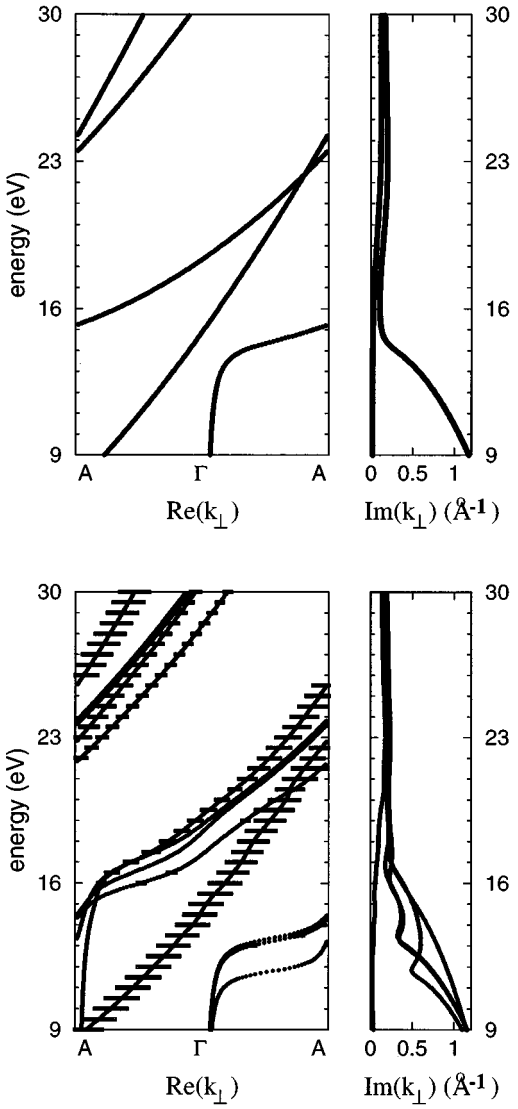

FIG. 3. The complex band structure of $TiSe_2$ for $\vec{k}_{\parallel}=0$. In the left-hand panels the real part Re($k_\perp$) is shown from bottom to top of the Brilloun zone. In the right-hand panels the imaginary part Im ($k_\perp$) is plotted. For the upper figure, damped plane waves were used, whereas the lower part was calculated with the quasilocal pseudopotentials. The length of the horizontal bars represents the transition probability, i.e., the squared modulus of the expansion coefficients t_n, see Eq. (7) in the photoemission computation.

found in terms of final states which are obtained from muffin-tin potentials. As the initial states used in those calculations are identical with ours, the difference has to be attributed solely to the complex band structure of the final states. Figure 3 shows the complex band structure for the quasilocal pseudopotential in comparison with that of damped plane waves. In view of the muffin-tin complex band structure plotted in Ref. 29, our pseudopotential result is more related to the plane-wave case than the muffin-tin result, though there are qualitative differences in the band splitting and bending. In particular, an enhanced fine structure appears in the imaginary part of $k_\perp$, which is important for the coupling of the bulk states to the vacuum. This similarity to the plane-wave case is expected to become apparent in the photocurrent too. The photocurrent with damped plane waves as final states displays only dispersive bands, the remaining two nondispersive ones being connected with a high density of states are completely suppressed. Therefore plane-wave features arising in the pseudopotential decrease the importance of the density of states in the photocurrent different from the muffin-tin case. A convincing agreement with the experimental data of Anderson, Manzke, and Skibowski[24] plotted in Fig. 2 can be stated. The variation of the relative intensities of photoemission peaks with photon energy and the relative intensities themselves are correctly reproduced by our numerical results. It should be added that the agreement with experiment seems to be better than that obtained with muffin-tin layer Korringa-Kohn-Rostoker final states in a former calculation of Pehlke *et al.*[25]. In particular, the dispersive structure is much more pronounced here. In our opinion the latter is a typical property of spectra calculated with pseudopotential, as opposed to muffin-tin potential, final states. The conduction-band wave functions in the rather low vacuum-ultraviolet photon regime seem to forbid the neglect of the interstitial potential in comparison with the strong spherical part.

As already stated in Ref. 30, the normal emission current from the surface parallel components of the light polarization vanishes for the free-electron-like damped plane waves as final states, i. e. only the identical representation of the initial states given mostly by the p_z orbitals survives. As a result, dispersive structures will be enhanced. Hence the slight similarity of the pseudopotential band structure with the plane-wave result explains our findings. From the convincing comparison with experiment, one would clearly favor the pseudopotential. Additionally, this is supported by the following arguments. First, it includes the interstitial potential. Second, a screening of the stronger muffin-tin potential seems to be physically necessary for the energetically high-lying final states. Third, because of its simplicity it is easy to calculate even off-normal photoemission spectra. The latter proved to be difficult to obtain in the past in the case when a muffin-tin potential for the final states is connected with an anisotropic potential for the initial states as forced by the anisotropic bindings of the layered crystals.

V. CONCLUSIONS

In concluding, the quasilocal pseudopotential derived from an *ab initio* nonlocal potential has proven its applicability to complex systems. It is constructed in a straightforward manner employing one adjustable parameter, the only *a posteriori* element of the scheme. Thus this method should be suitable for the wide class of materials for which the actual sophisticated pseudopotentials are made. Because of its simplicity it could be successfully used in a VLEED calculation for the determination of target current spectra. Additionally, in representing a nonspherical potential for the final states of photoemission, it is superior to the alternative use of standard muffin-tin potentials in covalent solids. It would be interesting to see whether this potential also works in the case of the bounded states of a surface system.

ACKNOWLEDGMENTS

We would like to thank M. Boehme for making TCS measurements available to us prior to publication, and S. Brodersen for test calculations on GaAs. This work was financially supported by the Bundesministerium für Bildung, Wissenschaft, Forschung und Technologie under Contract No. 05 605 FKA.

[1] A. L. Wachs, T. Miller, T. C. Hsieh, A. P. Shapiro, and T.-C. Chiang, Phys. Rev. B **32**, 2326 (1985).
[2] G. P. Williams, F. Cerrina, G. J. Lapeyre, J. R. Anderson, R. J. Smith, and J. Hermanson, Phys. Rev. B **34**, 5548 (1986).
[3] D. Straub, L. Ley, and F. J. Himpsel, Phys. Rev. B **33**, 2607 (1986).
[4] R. D. Bringans, R. I. G. Uhrberg, and R. Z. Bachrach, Phys. Rev. B **34**, 2373 (1986).
[5] J. Olde, K.-M. Behrens, H.-P. Barnscheidt, R. Manzke, M. Skibowski, J. Henk, and W. Schattke, Phys. Rev. B **44**, 6312 (1991).
[6] V. N. Strocov, Solid State Commun. **78**, 845 (1991).
[7] N. Sano and A. Yoshii, Phys. Rev. B **45**, 4171 (1992).
[8] J.-V. Peetz, W. Schattke, H. Carstensen, R. Manzke, and M. Skibowski, Phys. Rev. B **46**, 10 127 (1992).
[9] J. Henk, W. Schattke, H. Carstensen, R. Manzke, and M. Skibowski, Phys. Rev. B **47**, 2251 (1993).
[10] M. Reigrotzki, M. Stobbe, R. Redmer, and W. Schattke, Phys. Rev. B **52**, 1456 (1995).
[11] V. N. Strocov and H. I. Starnberg, Phys. Rev. B **52**, 8759 (1995).
[12] M. L. Cohen and T. K. Bergstresser, Phys. Rev. **141**, 789 (1966).
[13] M. C. Payne, M. P. Teter, D. C. Allan, T. A. Arias, and J. D. Joannopoulos, Rev. Mod. Phys. **64**, 1045 (1992).
[14] J. B. Pendry, J. Phys. C **2**, 2273 (1969).
[15] D. R. Hamann, M. Schlüter, and C. Chiang, Phys. Rev. Lett. **43**, 1494 (1979).
[16] G. B. Bachelet, D. R. Hamann, and M. Schlüter, Phys. Rev. B **26**, 4199 (1982).
[17] D. R. Hamann, Phys. Rev. B **40**, 2980 (1989).
[18] G. B. Bachelet, D. M. Ceperley, and M. G. B. Chiocchetti, Phys. Rev. Lett. **62**, 2088 (1989).
[19] W. M. C. Foulkes and M. Schlüter, Phys. Rev. B **42**, 11 505 (1990).
[20] J. R. Chelikowsky and M. L. Cohen, Phys. Rev. B **14**, 556 (1976).
[21] T. P. Humphreys and G. P. Srivastava, Phys. Status Solidi B **112**, 581 (1982).
[22] E. Clementi and C. Roetti, At. Data Nucl. Data Tables **14**, 177 (1974).
[23] J. A. Wilson and A. D. Yoffe, Adv. Phys. **18**, 193 (1969).
[24] O. Anderson, R. Manzke, and M. Skibowski, Phys. Rev. Lett. **55**, 2188 (1985).
[25] E. Pehlke, W. Schattke, O. Anderson, R. Manzke, and M. Skibowski, Phys. Rev. B **41**, 2982 (1990).
[26] P. J. Feibelman and D. E. Eastman, Phys. Rev. B **10**, 4932 (1974).
[27] J. Henk and W. Schattke, Comput. Phys. Commun. **77**, 69 (1993).
[28] D. Samuelsen and W. Schattke, Surf. Sci. **327**, 379 (1995).
[29] E. Pehlke and W. Schattke, J. Phys. C **20**, 4437 (1987).
[30] E. Pehlke and W. Schattke, Solid State Commun. **69**, 419 (1989).